Louisiana State University

LSU Digital Commons

9-28-2006

Dynamics of impurity and valence bands in Ga1-x Mnx As within the dynamical mean-field approximation

M. A. Majidi
University of Cincinnati

J. Moreno
University of Cincinnati

M. Jarrell
University of Cincinnati

R. S. Fishman
Oak Ridge National Laboratory

K. Aryanpour
University of Cincinnati

Follow this and additional works at: https://digitalcommons.lsu.edu/physics_astronomy_pubs

Recommended Citation

Dynamics of Impurity and Valence Bands in $Ga_{1-x}Mn_xAs$ within the Dynamical Mean Field Approximation

M. A. Majidi[1], J. Moreno[1,2], M. Jarrell[1], R. S. Fishman[3], and K. Aryanpour[1,4]

[1]*Department of Physics, University of Cincinnati, Cincinnati, Ohio 45221*
[2]*Department of Physics, University of North Dakota, Grand Forks, ND 58202*
[3]*Condensed Matter Sciences Division, Oak Ridge National Laboratory, Oak Ridge, Tennessee 37831 and*
[4]*Department of Physics, University of California, Davis, California 95616*
(Dated: October 16, 2018)

We calculate the density-of-states and the spectral function of $Ga_{1-x}Mn_xAs$ within the dynamical mean-field approximation. Our model includes the competing effects of the strong spin-orbit coupling on the $J = 3/2$ GaAs hole bands and the exchange interaction between the magnetic ions and the itinerant holes. We study the quasi-particle and impurity bands in the paramagnetic and ferromagnetic phases for different values of impurity-hole coupling, J_c, at the Mn doping of $x = 0.05$. By analyzing the anisotropic angular distribution of the impurity band carriers at $T = 0$, we conclude that the carrier polarization is optimal when the carriers move along the direction parallel to the average magnetization.

PACS numbers: 75.50.Pp,2.70.-c,5.10.-a,71.27.+a

The combined magnetic and semiconducting characteristics of ferromagnetic semiconductors make them excellent candidates for spintronic applications [1]. In particular, GaAs doped with Mn ($Ga_{1-x}Mn_xAs$) is promising as a spin-carrier injector in spintronic devices[2] due to its relatively high magnetic transition temperature [3] and its potential integration within the current semiconductor technology. However, the properties of magnetic semiconductors still need to be greatly optimized since practical uses demand magnetic transitions above room temperature and carrier polarization of at least 70% [1].

A realistic model which incorporates the relevant bands of the host material is crucial to guide the experimental efforts in the search for optimal magnetic semiconductors. In $Ga_{1-x}Mn_xAs$, the Mn ions are in the Mn^{2+} state with a half-filled d shell of total spin $S = 5/2$ [4, 5]. Since Mn^{2+} ions primarily replace Ga^{3+}, they contribute carrier holes to the p-like valence band. The strong spin-orbit interaction couples the $l = 1$ angular momentum to the electron spin ($s = 1/2$), resulting in a total spin $J = |l + s| = 3/2$ for the two upper valence bands and $J = |l - s| = 1/2$ for the split-off band [6]. Since the $J = 3/2$ bands are degenerate at the Γ point, an accurate model should include at least these two bands. However, a more realistic approach should incorporate the split-off and conduction bands as we discuss later.

Here, we continue our dynamical mean-field approximation (DMFA) [7, 8, 9, 10] study of the effects of strong spin-orbit coupling in $Ga_{1-x}Mn_xAs$[11]. While we previously examined the influence of the spin-orbit interaction on the ferromagnetic transition temperature T_c and the carrier polarization [11], we now focus on the density-of-states, the spectral function, and the dispersion of the quasi-particle and impurity bands. We also discuss the anisotropy of the spectra in the ferromagnetic phase and its influence on the transport properties.

Although the formation of the impurity band has been captured in previous DMFA studies [12], their model does not take into account the spin-orbit coupling and is unable to address the reduced carrier polarization within the impurity band. The DMFA describes the impurity band through quantum self-energy corrections which are not included in other mean-field theories. Because this method is non-perturbative, it allows us to study both the metallic and impurity-band regimes as well as both small and large couplings. Although the precise role played by the impurity band in $Ga_{1-x}Mn_xAs$ is still controversial, an array of experimental probes, such as angle-resolved photoemission [13], infrared spectroscopy [14, 15, 16], spectroscopic ellipsometry [17], scanning tunneling microscopy [18, 19], and photoluminescence techniques [20], display features characteristic of an impurity band.

We start with the Hamiltonian proposed in Ref. 11 and 21 :

$$H = H_0 - J_c \sum_{R_i} \mathbf{S}_i \cdot \hat{\mathbf{J}}(R_i) \ . \tag{1}$$

The first term incorporates the electronic dispersion and the spin-orbit coupling of the $J = 3/2$ valence holes within the spherical approximation[22]. The second term represents the interaction between the Mn spins and the valence holes [23], with J_c the exchange coupling and $\hat{\mathbf{J}}(R_i)$ the total $J = 3/2$ spin density of the holes at the site i of a Mn ion with spin $\mathbf{S}_i$. The relatively large magnitude of the Mn spin ($S = 5/2$) justifies its classical treatment.

Since the typical hole concentration is small (around 5%), the holes gather at the J=3/2 bands around the Γ point. This supports the use of the spherical approximation [22], for which the non-interacting Hamiltonian of pure GaAs is rotationally invariant. Hence, H_0 is diagonal in a *chiral* basis, $H_0 = \sum_{\mathbf{k},\gamma} \frac{k^2}{2m_\gamma} \tilde{c}^\dagger_{\mathbf{k}\gamma} \tilde{c}_{\mathbf{k}\gamma}$, where $\tilde{c}^\dagger_{\mathbf{k},\gamma}$

creates a chiral hole with momentum $\mathbf{k}$ parallel to its spin and $\mathbf{J} \cdot \hat{\mathbf{k}} = \pm 3/2$ or $\pm 1/2$. The two band masses $m_h \approx 0.5m$ and $m_l \approx 0.07m$ correspond to the heavy and light bands with $\gamma = \pm 3/2$ and $\pm 1/2$ respectively (m is the electron mass). Notice that for convenience we use the hole picture so that the valence bands have a minimum instead of a maximum at zero momentum. However, in displaying the results we reverse the sign back to accommodate the usual convention.

As discussed previously [11], the coarse-grained Green function matrix in the non-chiral fermion basis is

$$\hat{G}(i\omega_n) = \frac{1}{N} \sum_{\mathbf{k}} [i\omega_n \hat{I} - \hat{\epsilon}(k) + \mu\hat{I} - \hat{\Sigma}(i\omega_n)]^{-1}, \quad (2)$$

where N is the number of $\mathbf{k}$ points in the first Brillouin zone, μ is the chemical potential and $\hat{\epsilon}(k) = \hat{R}^{\dagger}(\hat{\mathbf{k}}) \frac{k^2}{2m_{\gamma}} \hat{R}(\hat{\mathbf{k}})$ is the dispersion in the spherical approximation. Here, $\hat{R}$ are spin $3/2$ rotation matrices that relate the fermion operator $c_{\mathbf{k}\gamma}$ to its chiral counterpart $\tilde{c}_{\mathbf{k}\gamma} = R_{\gamma\nu}(\hat{\mathbf{k}})c_{\mathbf{k}\nu}$, and repeated spin indices are summed. The mean-field function $\hat{\mathcal{G}}(i\omega_n) = [\hat{G}^{-1}(i\omega_n) + \hat{\Sigma}(i\omega_n)]^{-1}$ is required to solve the DMFA impurity problem. At a non-magnetic site, the local Green function equals the mean-field function $\hat{G}_{non} = \hat{\mathcal{G}}$, while the local Green function at a magnetic site is $\hat{G}_{mg}(i\omega_n) = [\hat{\mathcal{G}}^{-1}(i\omega_n) + J_c\mathbf{S} \cdot \hat{\mathbf{J}}]^{-1}$. To obtain this result, we treat disorder in a fashion similar to the *coherent potential approximation* (CPA) [24].

Now $\hat{G}_{mg}(i\omega_n)$ must be averaged over all possible spin orientations at the local site and over all possible impurity configurations on the lattice. The former is implemented by introducing the angular distribution function $P(\mathbf{S}) = \frac{\exp[-S_{eff}(\mathbf{S})]}{\mathcal{Z}}$, where $\mathcal{Z} = \int d\Omega_{\mathbf{S}} \exp[-S_{eff}(\mathbf{S})]$ and $S_{eff}(\mathbf{S})$ is the effective action of the system [25]

$$S_{eff}(\mathbf{S}) = -\sum_n \log\det\left[\hat{\mathcal{G}}(i\omega_n)(\hat{\mathcal{G}}^{-1}(i\omega_n) + J_c\mathbf{S} \cdot \hat{\mathbf{J}})\right]$$
$$\times e^{i\omega_n 0^+}. \quad (3)$$

The extra factor of $\hat{\mathcal{G}}(i\omega_n)$ in Eq.(3) is introduced to aid in convergence. If the Mn ions are randomly distributed with probability x, then the configurationally-averaged Green function reads $\hat{G}_{avg}(i\omega_n) = \left\langle \hat{G}_{mg}(i\omega_n) \right\rangle x + \hat{\mathcal{G}}(i\omega_n)(1-x)$.

When the magnetic order is along the z axis, $\hat{G}_{mg}$, $\hat{\mathcal{G}}$ and $\hat{\Sigma}$ are diagonal matrices and the angular distribution function depends only on the polar angle of the impurity spin: $P(\mathbf{S}) = P(\theta)$ [26]. In fact, $\hat{G}_{mg}$ can be written as a combination of the identity matrix, $\hat{I}$, $\hat{J}_z$, $\hat{J}_z^2$ and $\hat{J}_z^3$, where the coefficients are of order zero, one, two and three, respectively, of the magnetization: $\hat{G}_{mg} = O(1)\hat{I} + O(M)\hat{J}_z + O(M^2)\hat{J}_z^2 + O(M^3)\hat{J}_z^3$ [26]. Making use of

these results a new algorithm has been designed which dramatically reduces the computational time compared to our earlier work [11]. This improvement is due to the fact that the rotational symmetry of the model is explicitly broken by our choice of a preferential direction for the magnetization. Also, since the symmetry breaking is already incorporated in this algorithm, we no longer need a small magnetic field to break the symmetry along a magnetization axis [11].

To calculate dynamical quantities, we work in the real frequency domain, where the coarse-grained Green function matrix is

$$\hat{G}(\Omega) = \frac{1}{N} \sum_{\mathbf{k}} [\Omega\hat{I} - \hat{\epsilon}(\mathbf{k}) - \hat{\Sigma}(\omega)]^{-1} \quad (4)$$

with $\Omega = \omega + i0^+$.

Generally the Matsubara and real frequency Green functions need to be iterated simultaneously and averaged over the polar angle distribution $P(\theta)$. However, if we focus only on the paramagnetic phase ($T > T_c$) and the ferromagnetic ground state ($T = 0$) the angular distributions are known and self-consistency in the Matsubara domain is not necessary. In the paramagnetic phase, the angular distribution of the Mn spins is completely random so that $P(\theta) = 1/\pi$. In the $T = 0$ ferromagnetic ground state, the average impurity magnetization achieves its full value and $P(\theta) = \delta(\theta)$.

After the coarse-grained Green function is self-consistently calculated, the density-of-states is computed as

$$DOS(\omega) = -\frac{1}{\pi} \text{Im } Tr \, \hat{G}(\Omega) , \quad (5)$$

where Tr is the trace. Each of the diagonal elements of $-\frac{1}{\pi} \text{Im } \hat{G}(\Omega)$ is the projection of the density-of-states onto a state with fixed J_z component, i.e. $J_z = +3/2, +1/2, -1/2$, and $-3/2$.

We are also interested in the spectral function defined as

$$A(\mathbf{k}, \omega) = -\frac{1}{\pi} \text{Im } Tr \, [\Omega\hat{I} - \hat{\epsilon}(\mathbf{k}) - \hat{\Sigma}(\omega)]^{-1} . \quad (6)$$

The center of the quasi-particle peak in the spectral function represents the renormalized quasi-particle energy $\omega_{\mu}(\mathbf{k})$ ($\mu = 1, 2, 3, 4$), which can be obtained by solving the condition:

$$\text{Re } [\Omega\hat{I} - \hat{\epsilon}(\mathbf{k}) - \hat{\Sigma}(\omega)]_{diag} = 0 , \quad (7)$$

where the subscript $"diag"$ means that we first diagonalize the matrix, then solve the equation for each diagonal element.

We focus on the doping of $x = 0.05$, for which T_c is near the highest reported [3, 27, 28, 29, 30, 31, 32, 33]. Fig. 1 shows our results for the density-of-states for various values of J_c in the ferromagnetic phase (main panel) and the paramagnetic phase (inset). As J_c increases, states with
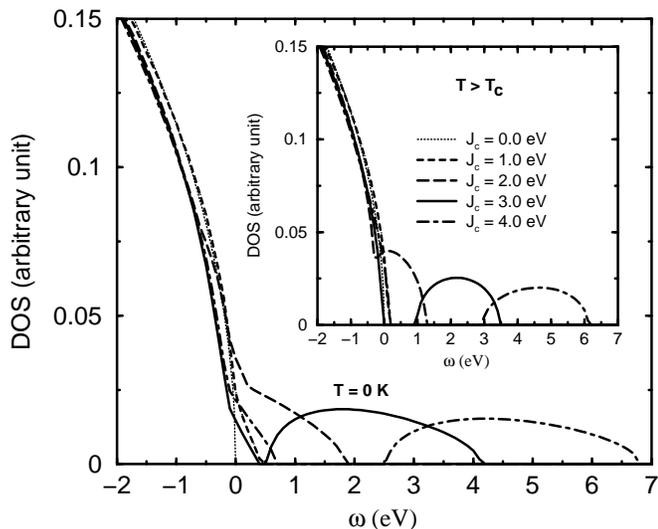
FIG. 1: Density-of-states for J_c=1.0, 2.0, 3.0, and 4.0 eV, at $T = 0$ (main panel) and $T > T_c$ (inset). The appearance of an impurity band is evident for $J_c > 2.0$ eV. The broader impurity band at $T = 0$, compared to that at $T > T_c$, indicates that lifetime of the bound-state holes decreases as the system becomes magnetically ordered.
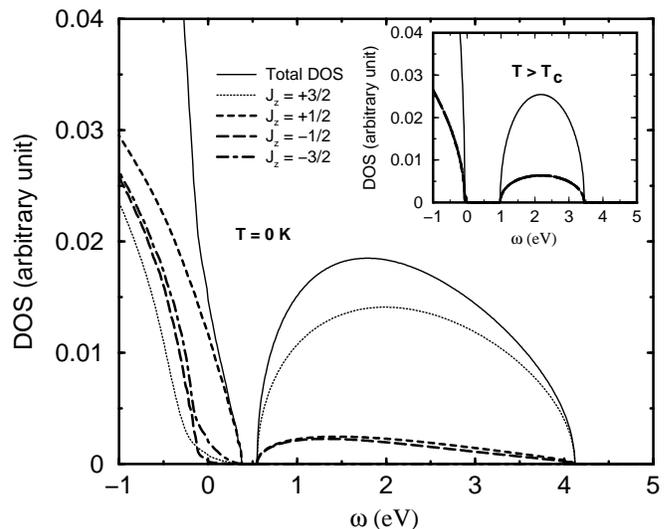

FIG. 2: Decomposition of the density-of-states in terms of J_z components, for $J_c = 3.0$ eV at $T = 0$ (main panel) and $T > T_c$ (inset). The chiral nature of the holes due to spin-orbit coupling mixes up states with different J_z components, making the total DOS only partially polarized at $T = 0$.

positive energy appear inside the semiconducting gap. These states correspond to the Zeeman splitting of the hole levels induced by the local impurity magnetization. For $J_c > 2.0$ eV an impurity band clearly appears. For $J_c = 3.0$ eV and $T = 0$, a second impurity band has started to form though it has not yet separated from the main band. We also observe a second impurity band appearing at positive energies in the paramagnetic phase when $J_c > 5.0$ eV (not shown in the graphs). The appearance of two impurity bands is consistent with the fact that the model includes two bands with $\mathbf{J} \cdot \hat{\mathbf{k}} = \pm 3/2$ and $\pm 1/2$.

As expected, the center of the impurity band shifts to higher energy as J_c increases. However, our predictions for the energy of the impurity band are too large. We believe that this is a consequence of excluding the conduction band from our model, since band repulsion with the conduction band pushes the impurity band to lower energies. We also notice that the impurity band in the ferromagnetic phase is broader than the one in the paramagnetic phase, confirming previous results [12, 25]. This suggests that the lifetime of the "bound-state" holes is shorter in the ferromagnetic phase because additional scattering events that exchange holes between impurities are required to maintain magnetic order. Hence, we will refer to the impurity-band states as *quasi-bound* states.

Next, we compare our density-of-states results with ARPES data in the paramagnetic phase of $Ga_{1-x}Mn_xAs$, $x = 0.035$ [13]. For this doping Okabayashi *et al.* observe an impurity band already well separated but not very far apart from the main band. A rough estimate for J_c of $2.0 - 3.0$ eV is the most suitable to describe the situation observed in the experimental setup. In the following

discussion we take $J_c = 3.0$ eV, though this value is an overestimate of the exchange coupling, to further explore the physical consequences of our model and the behavior of the impurity band.

Fig. 2 shows the decomposition of the DOS in terms of its J_z components for $J_c = 3.0$ eV. As expected, at $T > T_c$ all four components of J_z contribute equally to the total DOS, the electronic system is unpolarized. At $T = 0$, however, we see that the impurity band is not fully polarized, as would be expected for the double exchange model. In addition to the dominant $J_z = +3/2$ component, components with $J_z = +1/2$ and $-1/2$ are also present. This is clearly a consequence of the strong spin-orbit coupling, which mixes the $J_z = +3/2$ state with $J_z = \pm 1/2$ states. Previous DMFA studies[12] with coupling to only one carrier band captured the formation of the impurity band but were unable to address the effect of frustration on the carrier polarization.

Now we explore the spectral function of our model for $J_c = 3.0$ eV. Fig. 3 (a) shows the spectral function in the paramagnetic phase. Figs. 3(b) and (c) display the $T = 0$ spectrum along the direction parallel and perpendicular to the average magnetization, respectively. Notice two main effects on the energy levels: the valence band quasi-particle states (shown in main panels) are renormalized and the impurity band (shown in the blown-up insets) appears. Due to the localized nature of the impurity band states, their spectral weight extends over a large region in momentum space with typical values of the spectral function reduced by two orders of magnitude in comparison with the quasiparticles peaks.

The spectrum within the paramagnetic phase is isotropic, while it is obviously anisotropic in the ferromagnetic phase. For $J_c = 3.0$ eV all the quasi-particle
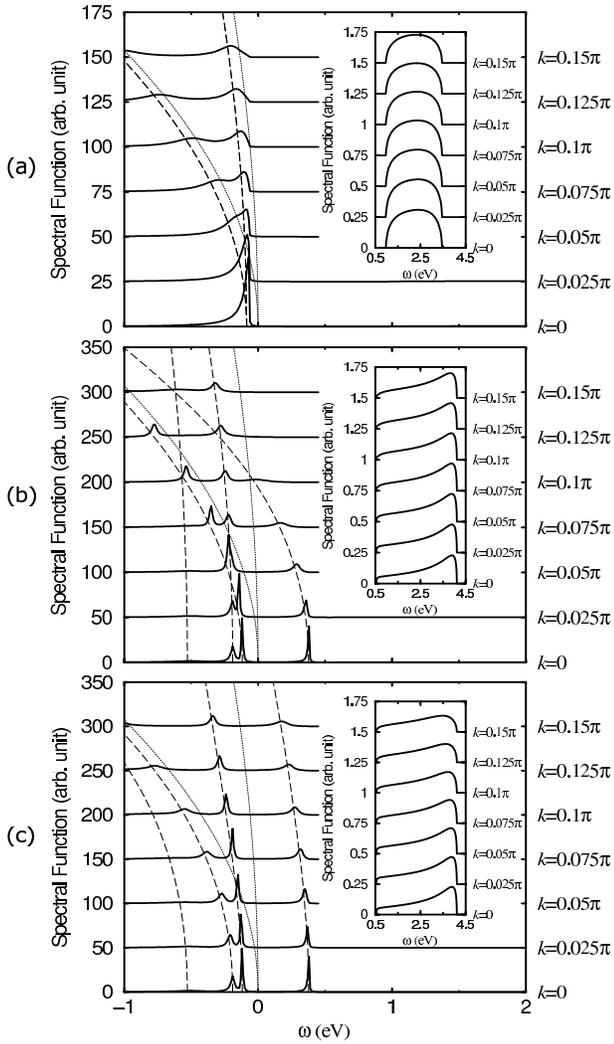
FIG. 3: Spectral functions near the center of the Brillouin zone for $J_c = 3.0$ eV at (a) $T > T_c$ along any direction, (b) $T = 0$ along the direction parallel and (c) perpendicular to the magnetization. Insets display a zoom of the impurity band region. Each spectral curve corresponds to a different value of the magnitude of the momentum k, as indicated at the right of the graphs, and the baseline of each spectrum is shifted proportionally to k for clarity. In the main panels the dashed curves represent the renormalized valence bands. For comparison, the valence bands of pure GaAs are also displayed (dotted curves). The scale in the insets is blown-up by a factor of 100 in (a) and 200 in (b) and (c).

FIG. 4: Variation of the J_z components of the impurity band spectral function for $J_c = 3.0$ eV and $T = 0$ ((a) $J_z = +3/2$, (b) $J_z = +1/2$, and (c) $J_z = -1/2$) as the magnitude of the momentum k changes from 0 (solid curve) to $k = 0.25\pi$ along the direction parallel (dotted curve) and perpendicular (long-dashed curve) to the average magnetization. Notice that the three graphs have different scales.

and the emerging impurity band. Also notice that the heavy and light quasiparticle bands are still degenerate at the Γ point.

In the ferromagnetic phase, the quasi-particle lines split into four. Since the finite magnetization competes with the chiral nature of the holes, the quasi-particle lines no longer correspond to well-defined chiral states. This is confirmed by Figs. 3(b) and (c) where the curvature (related to the effective mass) of the quasi-particle bands depends on the direction of the momentum. For the direction parallel to the average magnetization the spectrum of the quasiparticle band with $J_z = +1/2$ is shifted towards the semiconducting gap by approximately $0.4eV$ while the others bands are pushed towards negative energies. The positive shift in the $J_z = +1/2$ band is mainly due to the Zeeman splitting. The band repulsion between this band and the impurity states is very small since the impurity band hardly includes $J_z = +1/2$ quasiparticles with momentum parallel to the magnetization (see Fig. 4). On the other hand the $J_z = +3/2$ quasiparticle band shifts its spectrum by $\approx -0.2eV$ due to strong repulsion with the $J_z = +3/2$ states at the impurity band. However, for the direction perpendicular to the average magnetization the quasiparticle peak centered at $\omega \approx 0.4eV$ has $\mathbf{J} \cdot \hat{\mathbf{k}} = +3/2$ character. Since the impurity band on the perpendicular plane is formed mainly by $\mathbf{J} \cdot \hat{\mathbf{k}} = \pm 1/2$ states, the $\mathbf{J} \cdot \hat{\mathbf{k}} = +3/2$ quasiparticles do not suffer band repulsion.

Now examine the impurity band spectra in the insets. In the paramagnetic phase the impurity band does not show significant variation with $\mathbf{k}$, indicating strong localization of the bound-state holes. In the ferromagnetic phase, the variation with $\mathbf{k}$, although small, confirms that

lines track the peaks, and quasi particles are well defined. As expected in the paramagnetic phase, the states corresponding to $\mathbf{J} \cdot \hat{\mathbf{k}} = \pm 3/2$ and $\pm 1/2$ remain degenerate for all values of momentum. In this phase, the self-energy matrix is proportional to the identity [26], preserving $\mathbf{J} \cdot \hat{\mathbf{k}}$ as a good quantum number. The self energy just shifts the quasiparticle bands towards negative energies due to the band repulsion between the quasiparticle
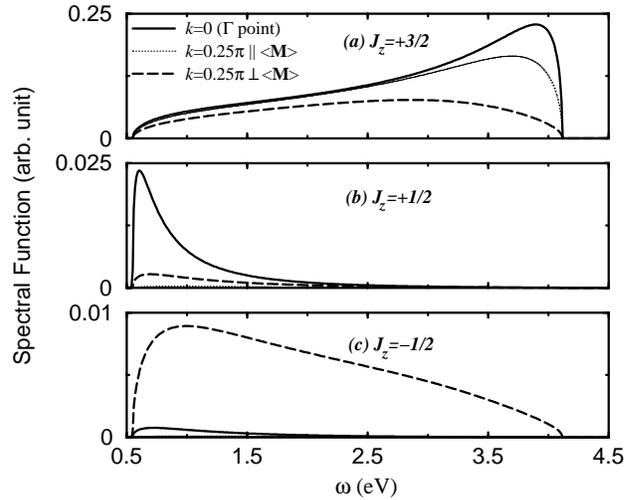
the bound-state holes are more mobile. Typical fillings leading to the highest critical temperatures correspond to values of the chemical potential inside the impurity band. Therefore, the transport properties rely on the impurity band rather than on the quasi-particle bands.

As demonstrated by Fig. 4 for the ferromagnetic phase, the impurity-band spectral function along the direction parallel to the magnetization is predominantly composed of $J_z = +3/2$ holes, whereas along the direction perpendicular to the magnetization, it is a mixture of $J_z = +3/2, +1/2$, and $-1/2$ states. This result suggests that the carrier polarization may be optimized by driving the current along the direction parallel to the magnetization. However, this may come with a price, since the carrier mobility is lower for the $J_z = +3/2$ heavy holes. Due to the mixing of heavy and light holes, the direction perpendicular to the magnetization may have higher mobility but lower carrier-spin polarization. Also notice that the $J_z = -1/2$ states participating in the local screening at the impurity band mostly display finite perpendicular momentum. This is the configuration most energetically favorable to avoid an exchange penalty while fulfilling spin-orbit constraints.

In conclusion, we have calculated the spectra of the renormalized valence bands and the impurity band of $Ga_{1-x}Mn_xAs$ within the DMFA. We compare our results with existing ARPES data for the paramagnetic phase [13]. From the anisotropy of the impurity band in the ferromagnetic phase, we predict that the direction parallel to the magnetization will produce the most polarized spin current, whereas the perpendicular direction may display higher conductivity with lower polarization. It would be interesting to be able to compare our results in the ferromagnetic phase with additional ARPES data.

[1] S. A. Wolf, D. D. Awschalom, R. A. Buhrman, J. M. Daughton, S. von Molnár, M. L. Roukes, A. Y. Chtchelkanova, D. M. Treger, Science **294**, 1488 (2001).

[2] Y. Ohno, D. K. Young, B. Beschoten, F. Matsukura, H. Ohno and D. D. Awschalom, Nature **402**, 790 (1999).

[3] For a recent review: A. H. MacDonald, P. Schiffer, and N. Samarth, Nature Materials **4**, 195 (2005).

[4] M. Linnarsson, E. Janzén, B. Monemar, M. Kleverman, A. Thilderkvist, Phys. Rev. B **55**, 6938 (1997).

[5] J. Okabayashi, A. Kimura, O. Rader, T. Mizokawa, and A. Fujimori, T. Hayashi and M. Tanaka, Phys. Rev. B **58**, R4211 (1998).

[6] J. S. Blakemore, J. Appl. Phys. **53**, R123 (1982).

[7] W. Metzner and D. Vollhardt, Phys. Rev. Lett. **62**, 324 (1989).

[8] E. Müller-Hartmann, Z. Phys. **B 74**, 507–512 (1989).

[9] T. Pruschke, M. Jarrell and J.K. Freericks, Adv. in Phys. **42**, 187 (1995).

[10] A. Georges, G. Kotliar, W. Krauth and M. Rozenberg, Rev. Mod. Phys. **68**, 13 (1996).

[11] K. Aryanpour, J. Moreno, M. Jarrell and R. S. Fishman, Phys. Rev. B **72**, 045343 (2005)

[12] A. Chattopadhyay, S. Das Sarma and A. J. Millis, Phys. Rev. Lett. **87**, 227202 (2001).

[13] J. Okabayashi, A. Kimura, O. Rader, T. Mizokawa, A. Fujimori, T. Hayashi and M. Tanaka, Phys. Rev. B **64**, 125304 (2001).

[14] E. J. Singley, R. Kawakami, D. D. Awschalom, and D. N. Basov, Phys. Rev. Lett. **89**, 097203 (2002).

[15] E. J. Singley, K. S. Burch, R. Kawakami, J. Stephens, D. D. Awschalom, and D. N. Basov, Phys. Rev. B **68**, 165204 (2003).

[16] K. S. Burch, E. J. Singley, J. Stephens, R. K. Kawakami, D. D. Awschalom, and D. N. Basov, Phys. Rev. B **71**, 125340 (2005).

[17] K. S. Burch, J. Stephens, R. K. Kawakami, D. D. Awschalom, and D. N. Basov, Phys. Rev. B **70**, 205208 (2004).

[18] B. Grandidier, J. P. Nys, C. Delerue, D. Stiévenard, Y. Higo, and M. Tanaka, Appl. Phys. Lett. **77**, 4001 (2000).

[19] T. Tsuruoka, N. Tachikawa, S. Ushioda, F. Matsukura, K. Takamura, and H. Ohno, Appl. Phys. Lett. **81**, 2800 (2002).

[20] V. F. Sapega, M. Moreno, M. Ramsteiner, L. Daweritz, and K. H. Ploog, Phys. Rev. Lett. **94**, 137401 (2005).

[21] G. Zaránd and B. Jankó, Phys. Rev. Lett. **89**, 047201 (2002).

[22] A. Baldereschi and N. O. Lipari, Phys. Rev. B. **8**, 2697 (1973).

[23] P. Kacman, Semicond. Sci. and Technol. **16**, R25 (2001).

[24] D. W. Taylor, Phys. Rev. **156**, 1017 (1967); P. Soven, *ibid.* **156**, 809 (1967); P. L. Leath and B. Goodman, *ibid.* **148**, 968 (1966).

[25] N. Furukawa, J. Phys. Soc. Japan **63**, 3214 (1994) and Proc. Conference on Physics of Manganites (1998) (available at http://xxx.lanl.gov/abs/cond-mat/9812066).

[26] J. Moreno, R. S. Fishman and M. Jarrell, cond-mat/0507487.

[27] H. Munekata, H. Ohno, S. von Molnár, A. Segmüller, L. L. Chang and L. Esaki, Phys. Rev. Lett. **63**, 1849 (1989).

[28] H. Ohno, H. Munekata, T. Penney, S. von Molnár and L. L. Chang, Phys. Rev. Lett. **68**, 2664 (1992).

[29] H. Ohno, A. Shen, F. Matsukura, A. Oiwa, A. Endo, S. Katsumoto and Y. Iye, Appl. Phys. Lett. **69**, 363 (1996).

[30] A. Van Esch, L. Van Bockstal, J. De Boeck, G. Verbanck, A. S. van Steenbergen, P. J. Wellmann, B. Grietens, R. Bogaerts, F. Herlach and G. Borghs, Phys. Rev. B. **56**, 13103 (1997).

[31] H. Ohno, Science **281**, 951 (1998).

[32] D. Chiba, K. Takamura, F. Matsukura and H. Ohno, Appl. Phys. Lett. **82**, 3020 (2003).

[33] K. W. Edmonds, P. Boguslawski, K. Y. Wang, R. P. Campion, S. N. Novikov, N. R. S. Farley, B. L. Gallagher, C. T. Foxon, M. Sawicki, T. Dietl, M. Buongiorno Nardelli, and J. Benholc, Phys. Rev. Lett. **92**, 037201 (2004).